

Sensitivity of Numerical Simulation of Early Rapid Intensification of Hurricane Emily (2005) to Cloud Microphysical and Planetary Boundary Layer Parameterizations

XUANLI LI AND ZHAOXIA PU

Department of Meteorology, University of Utah, Salt Lake City, Utah

(Manuscript received 4 September 2007, in final form 26 March 2008)

ABSTRACT

An advanced research version of the Weather Research and Forecasting (ARW) Model is used to simulate the early rapid intensification of Hurricane Emily (2005) using grids nested to high resolution (3 km). A series of numerical simulations is conducted to examine the sensitivity of the simulation to available cloud microphysical (CM) and planetary boundary layer (PBL) parameterization schemes. Results indicate that the numerical simulations of the early rapid intensification of Hurricane Emily are very sensitive to the choice of CM and PBL schemes in the ARW model. Specifically, with different CM schemes, the simulated minimum central sea level pressure (MSLP) varies by up to 29 hPa, and the use of various PBL schemes has resulted in differences in the simulated MSLP of up to 19 hPa during the 30-h forecast period. Physical processes associated with the above sensitivities are investigated. It is found that the magnitude of the environmental vertical wind shear is not well correlated with simulated hurricane intensities. In contrast, the eyewall convective heating distributions and the latent heat flux and high equivalent potential temperature (θ_e) feeding from the ocean surface are directly associated with the simulated intensities. Consistent with recognized facts, higher latent heat release in stronger eyewall convection, stronger surface energy, and high θ_e air feeding from the ocean surface into the hurricane eyewall are evident in the more enhanced convection and intense storms. The sensitivity studies in this paper also indicate that the contributions from the CM and PBL processes can only partially explain the slow intensification in the ARW simulations. Simulation at 1-km grid resolution shows a slight improvement in Emily's intensity forecast, implying that the higher resolution is somewhat helpful, but still not enough to cause the model to reproduce the real intensity of the hurricane.

1. Introduction

Owing to advancements in numerical modeling and data assimilation, much progress has been made in improving tropical cyclone (TC) forecasts. Over the past decade, TC track forecasts have been improved significantly. However, the intensity forecast still remains a challenging problem in both operational and research communities (Bender and Ginis 2000; Krishnamurti et al. 2005; Rogers et al. 2006). As addressed by Park and Zou (2004), TC intensity forecast errors were more than 50% higher than the errors regarded as the limit of predictability. Particularly, forecasting hurricane rapid intensification is even more challenging (Kaplan and DeMaria 2003) since it is plagued not only by the in-

adequate understanding of the physical processes of hurricane intensity change (Davis and Bosart 2002), but also by the improper physical parameterization in numerical models (Karyampudi et al. 1998; Houze et al. 2006).

The physical processes associated with TC intensifications have been investigated in numerous previous studies (e.g., Malkus 1958; Frank 1977; Willoughby 1988; Frank and Ritchie 1999; Montgomery et al. 2006). It has been recognized that the large-scale environmental conditions such as vertical wind shear and preexisting upper-level troughs, storm-scale vortex internal dynamics and thermodynamics, and air-sea interactions such as the ocean surface fluxes all play important roles (Davis and Emanuel 1988; DeMaria and Pickle 1988; Kuo et al. 1991; Merrill and Velden 1996; Willoughby and Black 1996; Bosart et al. 2000; Zhu et al. 2004). Among all these factors, the latter two are closely associated with the physical processes in numerical models. Therefore, physical parameterization schemes have

Corresponding author address: Dr. Zhaoxia Pu, Department of Meteorology, University of Utah, 135 S. 1460 E, Rm. 819, Salt Lake City, UT 84112-0110.
E-mail: zhaoxia.pu@utah.edu

a significant impact on accuracy forecasts of the hurricane intensity.

Previous studies indicated that hurricane intensity forecasts were greatly influenced by the representations of the cloud microphysical (CM) processes in numerical models. Willoughby et al. (1984) tested a warm-rain-only scheme and a mixed-ice-phase scheme in a two-dimensional nonhydrostatic model. They found that the final minimum central sea level pressure (MSLP) produced by the warm-rain-only CM scheme was 18 hPa lower (947 versus 965 hPa) than by the mixed-ice-phase scheme. An earlier and more rapid intensification within a shorter deepening time period was produced by the warm-rain-only CM scheme. However, the ice-microphysical processes initiated more mesoscale convective features. Stronger downdrafts were produced, which caused a later, slower development with a longer developing time period. With the same numerical model, Lord and Lord (1988) further investigated the impact of the ice-phase microphysics on the TC development. They found that more rapid microphysical conversion of cloud ice and cloud water to graupel prevented the horizontal spreading of the melting processes, and produced narrower and stronger updrafts and downdrafts. This stronger downdraft resulted in a slower storm intensification rate. With a three-dimensional hydrostatic model, Wang (2002) demonstrated that the use of warm-rain CM scheme causes a faster intensification rate of the storm than the mixed-phase scheme does, partly due to the stronger condensational heating in the warm-rain processes. They further suggested that a major prohibiting factor for the TC development is the strong downdrafts. Specifically, when the melting of snow and graupel and evaporation of rain were excluded, no downdraft and outer spiral rainbands were generated and the model produced the strongest storm with the most rapid intensification rate. Recently, Zhu and Zhang (2006) presented a pronounced sensitivity of the simulated intensity and inner core structure of Hurricane Bonnie (1998) to various CM processes in the fifth-generation Pennsylvania State University–National Center for Atmospheric Research (PSU–NCAR) Mesoscale Model (MM5) model. They indicated that the weakest storm can be produced by removing all ice particles from the CM processes due to greatly reduced latent heat release and much slower autoconversion and accretion processes. They also found that the cooling of melting ice particles and evaporating of cloud and rainwater had a breaking effect on the development of the hurricane. Hence, the most rapid development of the storm was produced when evaporation processes are removed.

In addition, numerical studies showed that the plan-

etary boundary layer (PBL) processes in the numerical model also have a significant influence on the simulated hurricane intensity (Anthes and Chang 1978). Braun and Tao (2000) showed that different PBL schemes in the MM5 model caused a difference of 16 hPa in the MSLP and 15 m s^{-1} in maximum surface wind (MSW) forecasts of Hurricane Bob (1991). The ratio of exchange coefficients of enthalpy and momentum in different PBL schemes has a large impact on the simulated storm intensity. Specifically, deeper intensity corresponded to larger exchange ratios. Davis and Bosart (2002) investigated the dynamics that govern the intensification and track of Tropical Cyclone Diana (1984) by varying the model cumulus parameterization, boundary layer treatment, sea surface temperature (SST), and horizontal grid spacing. They confirmed the importance of the model PBL scheme to the intensity forecast. However, both studies suggested that the simulated TC intensity does not solely depend on the PBL scheme. The complex interactions among PBL, CM, and storm dynamical processes play important roles in TC intensity change. McFarquhar et al. (2006) compared the roles of the PBL parameterization, condensation scheme, and CM processes in the simulation of Hurricane Erin (2001) using the MM5 model. They showed that the PBL process was crucial in the forecast of Erin's final intensity, while the condensation scheme could also have a major impact. More importantly, even small changes in a single microphysical parameter could cause notable differences in the intensity forecast.

Although most of the aforementioned sensitivity studies investigated the roles of physical parameterization schemes in the numerical simulations of hurricanes, it is still not clear how and why the physical parameterizations influence the simulated storm development because of the complex interactions among the physical processes in numerical models. In addition, little progress has been made in the understanding of the rapid intensification of hurricanes. In this study, we will investigate the sensitivity of numerical simulations of early rapid intensification of Hurricane Emily (2005) to various CM and PBL parameterization schemes in a short-range numerical simulation, using the new-generation mesoscale community model, Weather Research and Forecasting (WRF) Model. The purposes of this study go beyond a case study with this model to complement previous sensitivity studies. More importantly, we intend to understand the physical processes through which the different model physical parameterization schemes influence the simulated intensification of Hurricane Emily.

The paper is organized as follows. Section 2 includes a brief overview of Hurricane Emily and a description

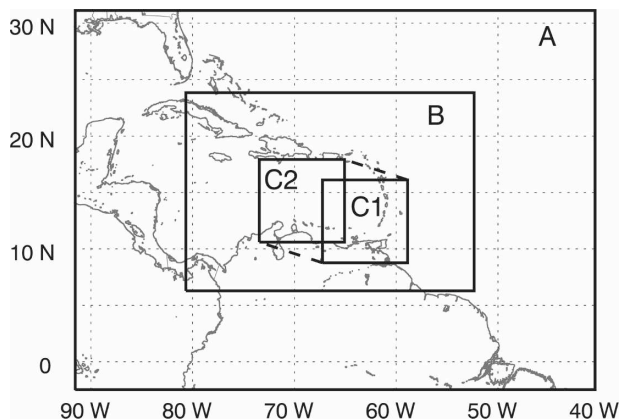


FIG. 1. The locations of the model domains for the numerical simulations of Hurricane Emily (2005). Domain A is the 27-km grid and domains B and C are the nested 9- and 3-km grid, respectively. Domain C moved from C1 to C2 at 15 h.

of the numerical model and experimental design. Numerical results examining the sensitivity of various CM and PBL schemes to simulated hurricane intensity, and the physical processes associated with these sensitivities are analyzed in sections 3, 4, and 5. Concluding remarks are drawn in section 6.

2. Simulation description

a. Summary of Hurricane Emily (2005)

Hurricane Emily (2005) formed on 10 July and dissipated on 21 July 2005. It crossed the Yucatan Peninsula and made landfall in northeastern Mexico. With the MSW of 72 m s^{-1} and MSLP of 929 hPa, Emily is the strongest and the longest-lived hurricane ever in the month of July in the Atlantic Ocean basin (Franklin and Brown 2006).

In this study, numerical simulations are concentrated on the early rapid intensification period of Hurricane Emily during 0600 UTC 14 July to 0600 UTC 15 July when the observed MSLP changed from 991 to 952 hPa. During this 24-h period, Emily intensified rapidly from a tropical storm to a category-4 hurricane on the Saffir–Simpson hurricane scale with the extreme deepening rate of about 2 hPa h^{-1} . This rapid deepening rate and the unprecedented early formation time of such an intense storm make Hurricane Emily an interesting case to study.

b. Model setup

An advanced research version of the Weather Research and Forecasting [Advanced Research WRF (ARW)] Model (version 2.0) is used to conduct numerical simulations of the early rapid intensification of Hur-

TABLE 1. The dimensions, grid spaces, and time steps for model domains.

Domain	Dimension ($x \times y \times z$)	Grid space	Time step
A	$190 \times 140 \times 31$	27 km	120 s
B	$340 \times 220 \times 31$	9 km	40 s
C	$301 \times 271 \times 31$	3 km	13.3 s

ricane Emily. The ARW model is a recently developed next-generation mesoscale numerical weather research and forecasting system. In addition to its dynamic core with advanced numerical methods, the model carries multiple physical options for cumulus, CM, PBL, and radiation physical processes. For a more detailed description of ARW, the reader is referred to Skamarock et al. (2005).

A two-way interactive, three-level nested grid technique is employed to conduct the multiscale simulations with the ARW model. Figure 1 shows the location of model domains and Table 1 lists the specifications for the model domains. The outer domains A and B (27- and 9-km grid spacings) integrate from 1800 UTC 13 July to 1200 UTC 15 July 2005 with data assimilation (see section 2b) during the first 12 h of the simulation. The innermost domain C (3-km grid spacing) starts at 0600 UTC 14 July 2005 and moves to keep the storm near the center of the domain (increment from C1 to C2 as shown in Fig. 1). The model vertical structure comprises 31 σ levels with the top of the model set at a pressure of 50 hPa, where $\sigma = (p_h - p_{ht}) / (p_{hs} - p_{ht})$ while p_h is the hydrostatic component of the pressure, and p_{hs} and p_{ht} refer to values of the pressure along the surface and top boundaries, respectively.

The model physics options are the same for all three domains except that no cumulus parameterization is included for the 3-km domain. The Rapid Radiative Transfer Model (RRTM) longwave radiation (Mlawer et al. 1997) and Dudhia shortwave radiation schemes (Dudhia 1989) are adopted. The Grell–Devenyi ensemble cumulus scheme (Grell and Devenyi 2002), which has a better performance in the simulation of Hurricane Emily in the previous study (Li and Pu 2006), is used for the 27- and 9-km grid spacings. The PBL and CM schemes vary in different experiments (Tables 2 and 4).

c. Initial and boundary conditions

The boundary conditions for the ARW model simulations are derived from the National Centers for Environmental Prediction's (NCEP) final analysis (FNL) field at $1^\circ \times 1^\circ$ resolution. The model initial conditions are generated by using a WRF three-dimensional variational data assimilation (3DVAR) system, which was

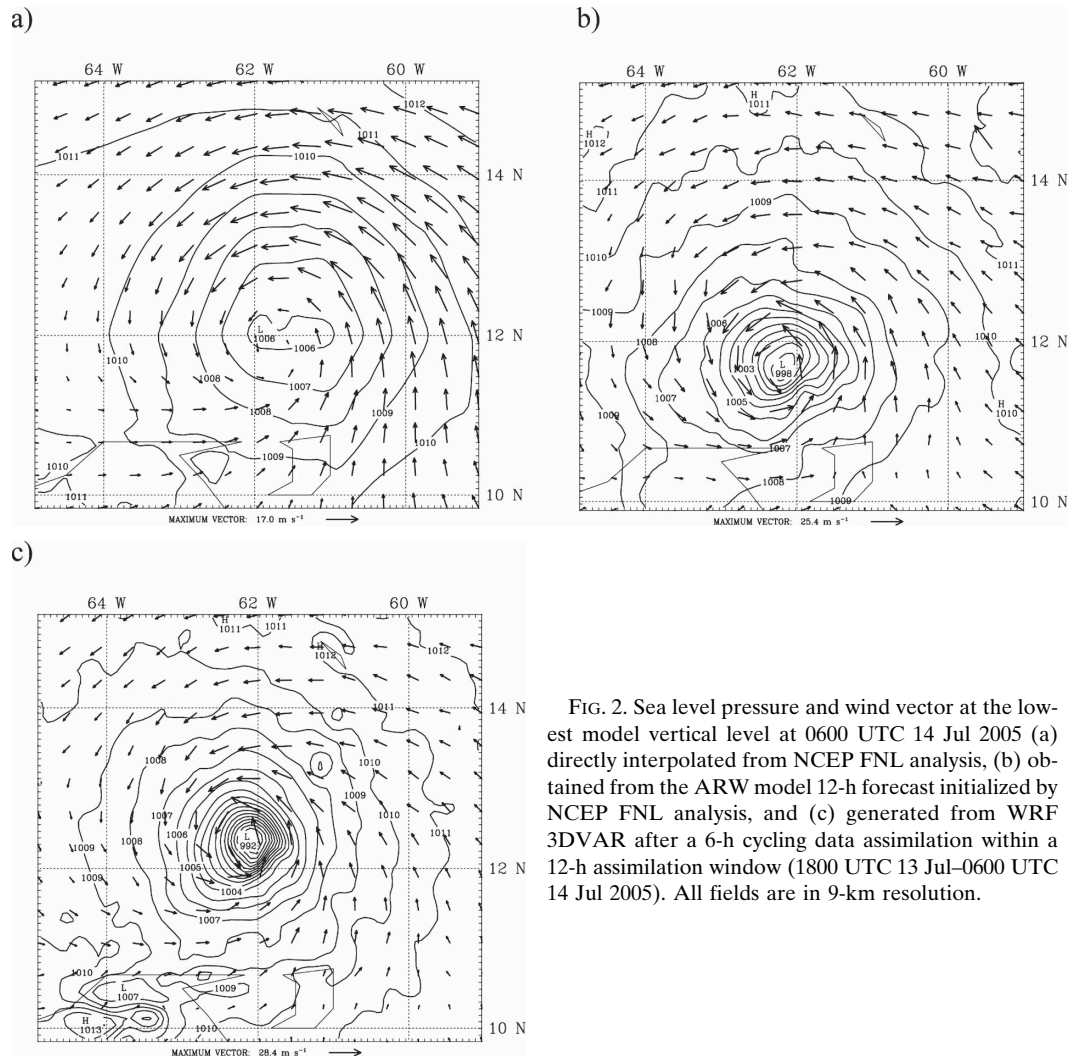


FIG. 2. Sea level pressure and wind vector at the lowest model vertical level at 0600 UTC 14 Jul 2005 (a) directly interpolated from NCEP FNL analysis, (b) obtained from the ARW model 12-h forecast initialized by NCEP FNL analysis, and (c) generated from WRF 3DVAR after a 6-h cycling data assimilation within a 12-h assimilation window (1800 UTC 13 Jul–0600 UTC 14 Jul 2005). All fields are in 9-km resolution.

developed at the National Center for Atmospheric Science (NCAR) based on the MM5 3DVAR system (Barker et al. 2004). The *Geostationary Operational Environmental Satellite 11 (GOES-11)* rapid scan atmospheric motion vectors, the Quick Scatterometer (QuikSCAT) ocean surface vector winds, and aircraft dropwindsonde data, collected during the National Aeronautics and Space Administration (NASA) Tropical Cloud Systems and Processes (TCSP) experiment (Halverson et al. 2007), are assimilated into the ARW model with the available conventional data in both 27- and 9-km grids in a 6-hourly cycling data assimilation within the 12-h assimilation window (1800 UTC 13 July–0600 UTC 14 July 2005). Detailed methodology for data assimilation can be found in Pu et al. (2008). After the data assimilation, the initial conditions for 3-km grid spacing are interpolated from 9-km grids. With current WRF 3DVAR, initialization is only done

for regular analysis variables such as horizontal and vertical wind components, temperature, moisture, and pressure. No microphysical property initialization is included in the data assimilation. Therefore, the microphysical properties are spun up by model physics once the model integration starts. In other words, when all simulations begin at the same initial conditions, the differences in the simulations will solely rely on the dynamics and physics options used in the ARW model.

Data assimilation has improved the initial condition of the ARW model. To show the accuracy of the initial conditions from the data assimilation, Fig. 2 compares the sea level pressure and wind vector at the lowest model vertical level at 0600 UTC 14 July 2005 obtained from 1) interpolation of NCEP FNL global analysis (a common way to start mesoscale numerical simulations), 2) 12-h ARW model simulation initialized by NCEP FNL analysis, and 3) analysis field from WRF 3DVAR

TABLE 2. List of the cloud microphysics sensitivity experiments and their physics options.

Expt	Cloud microphysics option
KS	Kessler warm-rain scheme
LIN	Purdue Lin scheme
WSM3	WSM three-class simple ice scheme
WSM5	WSM five-class mixed phase scheme
WSM6	WSM six-class graupel scheme
FERR	Eta Ferrier scheme

after a 6-hourly cycling data assimilation within a 12-h assimilation window (1800 UTC 13 July–0600 UTC 14 July 2005). At that time, Emily is observed as a nearly category 1 hurricane with MSLP of 991 hPa and MSW of 39 m s^{-1} . As in Fig. 2, both the NCEP FNL analysis and the ARW simulation do not produce storms with an accurate intensity. Specifically, the FNL analysis (Fig. 2a) produces a tropical storm with MSLP of 1003 hPa. The ARW simulation (Fig. 2b) performs better than direct interpolation from FNL analysis, but the simulated MSLP is 998 hPa, which is still 7 hPa weaker than the observed intensity. With data assimilation (Fig. 2c), the MSLP of Emily reached 992 hPa, which is only 1 hPa shallower than the observed intensity. The MSW is also very close to the observed one.

With the improved initial conditions provided by WRF 3DVAR, high-resolution (3 km) numerical simulations are conducted to examine the sensitivity of the numerical simulation of Hurricane Emily's early rapid intensification to the CM and PBL parameterizations. Unless otherwise specified, all results discussed thereafter are from the 3-km grid spacings.

3. Sensitivity to cloud microphysical schemes

Experiments are conducted with six different CM schemes (listed in Table 2) in the ARW model. These CM schemes differ in their complexity and hydrometeor species. Specifically, the Kessler scheme (Kessler 1969) is a simple warm-cloud scheme. It only includes three species of hydrometeors: water vapor, cloud water, and rainwater. The Purdue Lin scheme (LIN), which is based on Lin et al. (1983) with some modifications (Chen and Sun 2002), is a relatively more sophisticated scheme. It includes six classes of hydrometeors: vapor, cloud water, rain, cloud ice, snow, and graupel. The WRF single-moment three-class (WSM3) scheme (Hong et al. 2004) is the so-called simple ice scheme. It includes three categories of hydrometeors: vapor, cloud water–ice, and rain–snow. The cloud ice and snow exist when the temperature is less than or equal to the freezing point; otherwise, cloud water and rain are present. The WRF single-moment five-class

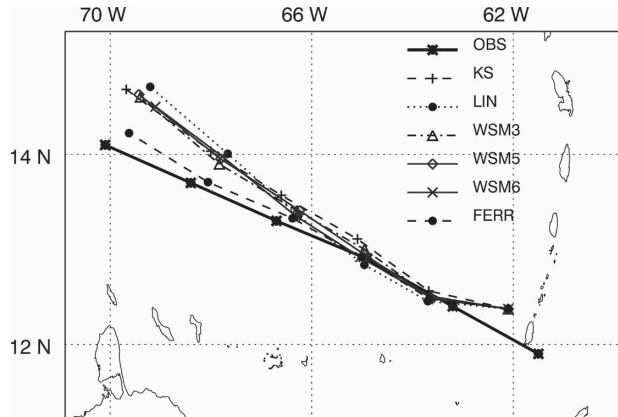


FIG. 3. Forecasts of the hurricane track from model simulations during 0600 UTC 14 Jul–1200 UTC 15 Jul 2005, compared with the National Hurricane Center best-track data. Center locations along the tracks are indicated every 6 h.

(WSM5) scheme (Hong et al. 2004) is a mixed-phase scheme. It includes five categories of hydrometeors: vapor, rain, snow, cloud ice, and cloud water. Supercooled water can exist in this scheme. The WRF single-moment six-class (WSM6) scheme (Hong and Lim 2006) is an extension of the WSM5 scheme with graupel included. Both the LIN and WSM6 schemes include six categories of hydrometeors, but they are different in the ice microphysical processes. The WSM6 scheme improved the number concentration, accretion, and ice nucleation in the cloud ice formation processes (Hong and Lim 2006). The Eta Ferrier scheme (FERR; Rogers et al. 2001) is different from all above schemes because it predicts changes in water vapor and total condensate. The total condensate combines all hydrometeor fields: cloud water, rain, cloud ice, and precipitating ice (snow and graupel). For all experiments in this section, the Yonsei University (YSU) PBL schemes are adopted.

a. Track

Figure 3 compares the track forecasts from different experiments with the National Hurricane Center (NHC) best track. The corresponding track errors are also listed in Table 3. In the first 18 h (0600 UTC 14 July–0000 UTC 15 July 2005), the track forecasts in different experiments are quite similar. All simulations reproduce the observed west-northwestward storm movement with the average speed of 7 m s^{-1} . In the last 12 h (0000 UTC 15 July–1200 UTC 15 July 2005), FERR produces the best-track forecast for Emily with the smallest track errors among all experiments. Overall, except FERR, the track forecast of Hurricane Emily is not very sensitive to the CM schemes in the ARW model.

TABLE 3. Track errors (km) for the microphysics sensitivity experiments during 0600 UTC 14 Jul–1200 UTC 15 Jul 2005.

Forecast hours	KS	LIN	WSM3	WSM5	WSM6	FERR
0 h	73 km					
6 h	66 km	68 km	66 km	65 km	65 km	65 km
12 h	31 km	16 km	16 km	11 km	15 km	11 km
18 h	40 km	43 km	43 km	43 km	43 km	32 km
24 h	52 km	68 km	63 km	58 km	63 km	45 km
30 h	62 km	97 km	78 km	78 km	94 km	43 km

b. Intensity

Figure 4 compares the simulated and observed MSLP and MSW during 0600 UTC 14 July–1200 UTC 15 July 2005. Although all experiments start from the same initial conditions, the intensity forecasts are significantly different in various experiments. At the end of the 30-h forecasts, the simulated intensities range from a 6-hPa overdeepening in MSLP (or 11 m s^{-1} in MSW) to a 23-hPa underdeepening in MSLP (or 16 m s^{-1} in MSW). In addition, even though the initial hurricane intensity matches well with the observed intensity, none of the simulations capture the real rapid deepening rate during the first 24-h forecasts. Only when the storm experiences a weakening in the last 6 h did the Kessler scheme (KS) catch up with the observed MSLP and produced an overdeepening in MSLP; at the same time, the model fails to predict the weakening of the hurricane in almost all experiments. Since the observed evidence about this weakening in the last 6-h simulation period is generally lacking and our main goal is to discuss the short-range forecast of the rapid intensification of Hurricane Emily, most discussions in this paper focuses on the first 24 h of the simulations.

Overall, only slight differences in storm intensity are found among all experiments in the first 9 h of the simulations. Afterward, the differences in the simulated intensities increase with time. Specifically, with the warm-rain KS, the model produces the earliest and quickest intensification among all experiments with an extreme deepening rate of 3 hPa h^{-1} . This result agrees with the numerical simulations from Lord et al. (1984) and Wang (2002) as mentioned in the introduction. In contrast, the model produces weaker storms with the ice-phased CM schemes. In particular, WSM3 generates the shallowest storm and the slowest deepening rate. At the end of the simulation, WSM3 only produces a category 1 hurricane with MSLP of 987 hPa. WSM5 produces a storm with MSLP at 975 hPa, which is 12 hPa deeper than that in WSM3. The difference in the intensity forecast between WSM3 and WSM5 can be attributed to the exclusion and inclusion of the

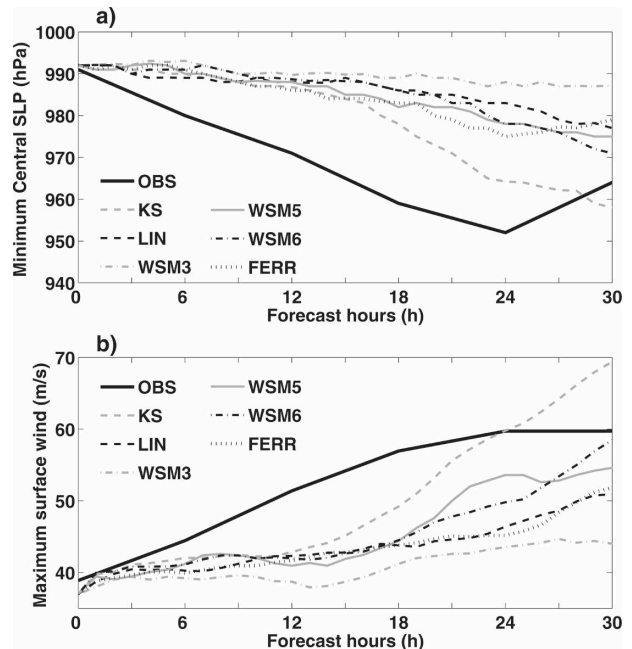


FIG. 4. Time series of (a) MSLP (hPa) and (b) maximum surface wind speed (m s^{-1}) from the National Hurricane Center best-track data and the numerical simulations during 0600 UTC 14 Jul–1200 UTC 15 Jul 2005.

mixed-phase microphysical processes, as well as the corresponding different ways in representing the melting–freezing processes. Furthermore, a deeper intensity is produced by WSM6 due to the inclusion of graupel into the CM processes. At the end of the simulation, the MSLP forecast from WSM6 is 4 hPa closer to that of the observation than the forecast from WSM5. When compared with WSM6, LIN produces a similar trend but slower deepening rate, mainly reflecting the different dynamical and thermal responses in the numerical model to the different CM processes in the two schemes. At the end of the simulation, the MSLP produced by LIN is 6 hPa shallower than that from WSM6. The simulated MSLP in FERR dropped by 17 hPa in the first 24 h, and followed by a slight weakening in the last 6 h of the simulation. The FERR scheme is the only scheme that causes the model to reproduce the observed weakening event during the last 6 h although the simulated storm intensity is much weaker than the observed one.

c. Hydrometeors and precipitation

Since the fundamental differences among all CM schemes are the magnitudes and distributions of hydrometeors, it is desirable to examine first the evolution of the cloud hydrometeors in different experiments. Figure 5 compares the time series of the total-column-

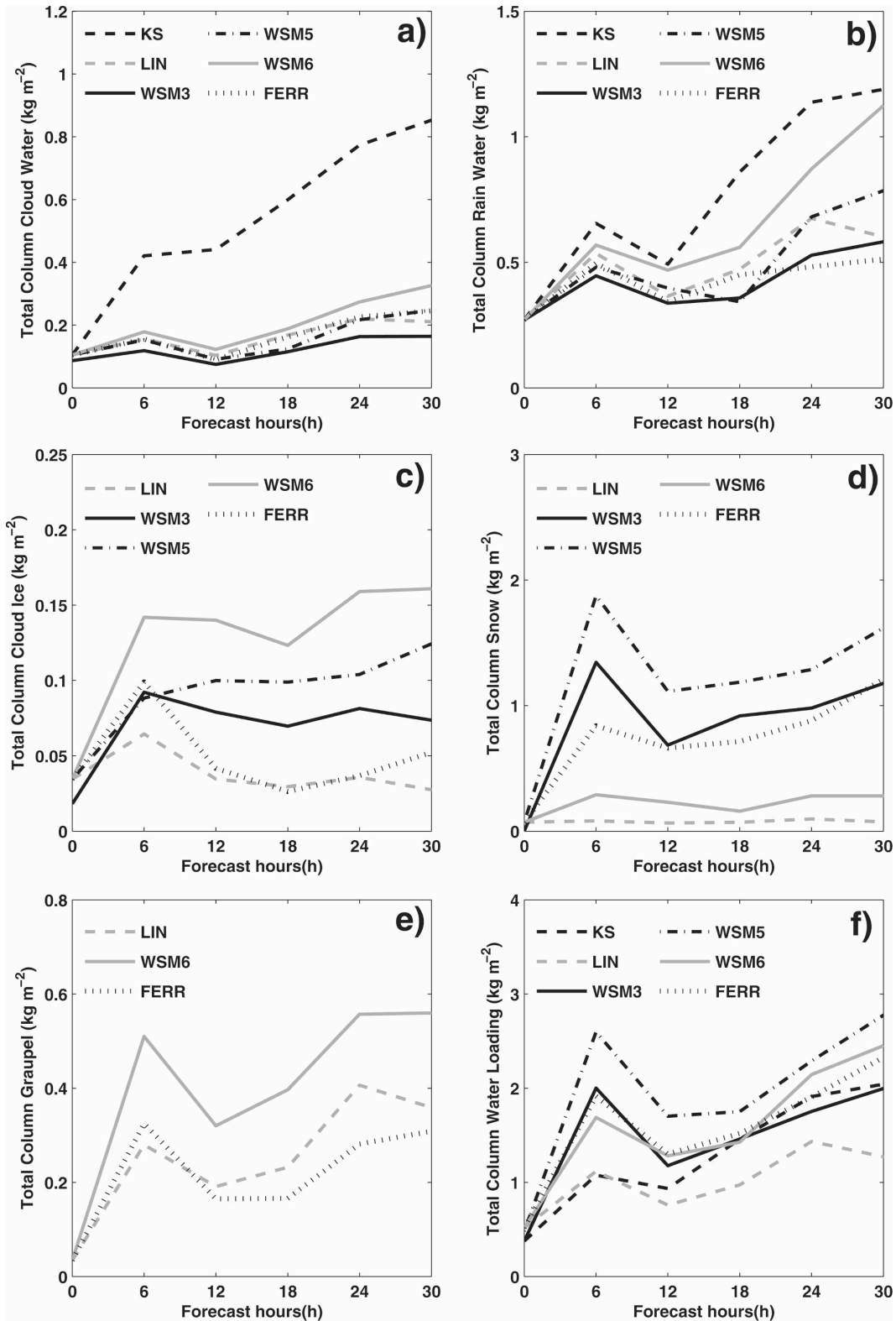


FIG. 5. Time series of the of the area average (kg m^{-2} ; within the 250-km radius from the storm center) of the total-column-integrated (a) cloud water, (b) rainwater, (c) cloud ice, (d) snow, (e) graupel, and (f) total water loading obtained from the different simulations during 0600 UTC 14 Jul–1200 UTC 15 Jul 2005.

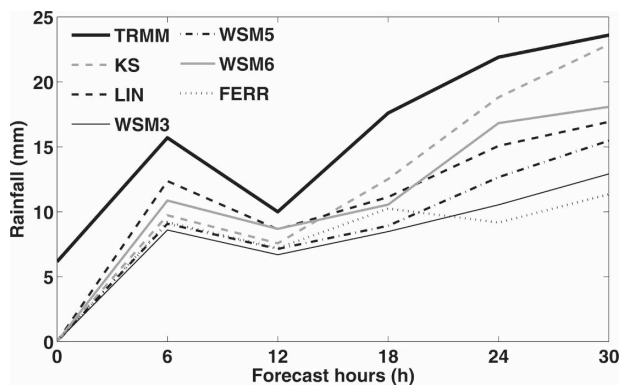


FIG. 6. Time series of the area-averaged 6-h accumulated rainfall (mm; averaged within the 250-km radius from the storm center) obtained from the different simulations and the TRMM 3B42 products during 0600 UTC 14 Jul–1200 UTC 15 Jul 2005.

integrated cloud water, rainwater, cloud ice, snow, graupel, and total water loading (the sum of cloud water, cloud ice, rainwater, snow, and graupel; kg m^{-2}) averaged over storm core region (within the 250-km radius from the storm center) from all experiments. In general, the amounts of total column hydrometeors are quite different in different experiments. Specifically, KS remarkably differs from the other experiments by producing much more cloud and rainwater during the whole simulation period (Figs. 5a,b). WSM3 generates the least amount of rain and cloud water. WSM5 produces the most amount of total water loading among all experiments during the whole simulation period, mainly in the form of snow (Figs. 5d,e). WSM6 generates larger amounts of column-integrated cloud ice and graupel than FERR and LIN.

The storm-induced precipitation is highly related to the magnitudes and distributions of cloud hydrometeors. Significant differences in rainfall distribution, rainfall intensity, and rainband structure are seen in different experiments (figure not shown). To make a quantitative comparison, Fig. 6 illustrates the time series of 6-h accumulated rainfall averaged over the storm core region (within the 250-km radius from the storm center) from different experiments compared with the real-time rainfall products (3B42; Huffman et al. 2007) from NASA's Tropical Rainfall Measuring Mission (TRMM). Overall, the simulations of the rainfall amounts capture the trend in the observed rainfall. However, almost all simulations consistently underestimate the magnitudes rainfall during the whole simulation period. This underestimation may be related to weaker storms produced by the numerical simulations. In addition, overall changes in the magnitudes of the precipitation seem to have good correlations with the simulated storm intensity changes (Fig. 4) and the

trends of the evolution of the cloud hydrometeors, especially for rainwater (Fig. 5b). For instance, the strongest storm in KS corresponds to the largest amount and the most rapidly increasing rate of accumulated rainfall and total-column cloud water and rainwater. The weaker storm in WSM3 corresponds to the relative smaller amount of precipitation and the total-column rainwater.

4. Storm inner-core structures, vertical wind shear, and surface energy transport

Section 3 showed that the sensitivity of simulated hurricane intensities is closely associated with the different distributions of cloud hydrometeors and precipitation over the storm cores. In this section, we will discuss the physical processes by which these two factors influence the simulated storm structure and its development.

The physics relating to the development and maintenance of TCs have been well indicated by numerous previous studies. A typical example regarding to the development of the TC inner core is a conceptual model drawn by Willoughby (1988) (shown in Fig. 7). This model clearly explains the dynamic and physical mechanism of TCs. As indicated by this conceptual model, a TC is a thermodynamic heat engine. This heat engine works in an in-up-and-out pattern, which is the so-called hurricane secondary circulation. At low levels of the atmosphere, air flows toward the low pressure at the storm center. This inward air absorbs heat and moisture from the surface of the warm tropical oceans. The absorption of energy and moisture can increase the conditional instability in boundary layer and enhance the potential for more intense vertical motion in the storm eyewall. Thus, energy from the ocean surface is the primary energy source for the updrafts in the eyewall. During the convection occurring in the storm eyewall, a great amount of latent heat will be released by condensation and fusion processes. This strong latent heating is the direct force that drives the eyewall convection and the secondary circulation of a hurricane, which causes the storm to maintain itself and develop further. At upper levels of the atmosphere, outflowing air exists to compensate the inflow at the low troposphere.

According to Willoughby's conceptual model, the latent heat release in the eyewall convection is the major energy source for hurricane development, it is closely related to the CM processes and the formation of cloud hydrometeors. To investigate further the impact of the different CM schemes on numerical simulations, the vertical distributions of cloud hydrometeors, convective

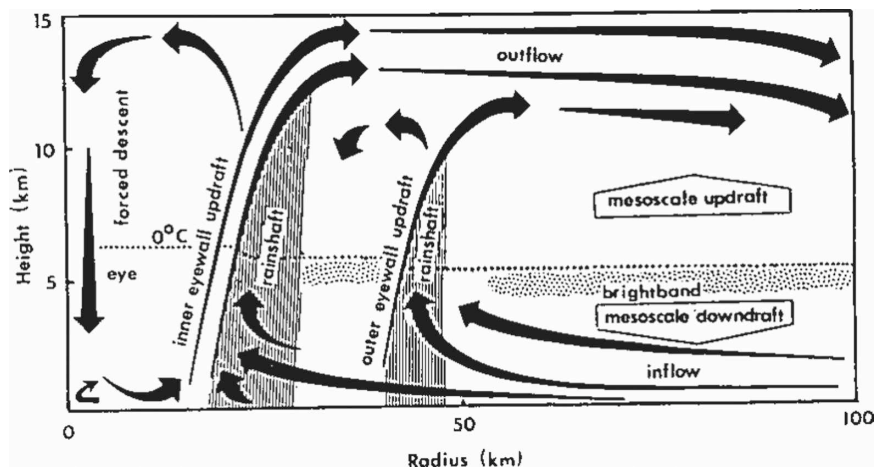


FIG. 7. Schematic illustration of the dynamics of the tropical cyclone core (Courtesy of Willoughby 1988).

heating rates, vertical motion, divergence, and the fluxes from the ocean surface over the storm core region are examined for all simulations at 0600 UTC 15 July 2005, when simulated storms obtain further development in most numerical experiments.

a. Vertical distributions of hydrometeors and the convective heating rate

Figure 8 compares the vertical profiles of cloud water, rainwater, cloud ice, snow, and graupel mixing ratio averaged over the storm core region (within the radius of 250 km from the storm center) at 0600 UTC 15 July 2005. Figure 9 shows the radius–height distribution of the convective heating rate. The figures indicate markedly different vertical structures of hydrometeors and corresponded convective heating rates over the storm eyewalls.

Significant amounts of cloud water and rainwater present in the whole column in KS (Figs. 8a,b and 5a,b), corresponding to the stronger convective heating rate with the maximum value of 24 K h^{-1} near 400 hPa at the storm eyewall (Fig. 9a). The rainwater is greatest in the low to midtroposphere, but the cloud water reaches its peak in the upper troposphere since the cloud water cannot be efficiently converted into precipitation there (Grabowski 1998). With no ice particles in the clouds, the melting effect is not included in the warm-rain KS. As suggested by Zhu and Zhang (2006), removing the melting effect from the CM processes may result in relative warmer and moister air around the TC vortex. This warmer, moister air can help to generate larger latent heat release over the storm core region, which benefits the development of the TC. This may be one of the reasons for the stronger storm produced in KS.

Since the WSM3 CM scheme defines cloud water

(cloud ice) and rainwater (snow) according to temperature above (below or equal to) zero, the melting and freezing processes in WSM3 occur instantaneously around the melting level (Hong and Lim 2006). Due to this limitation, WSM3 produces relatively smaller amounts of rainwater (Figs. 8b and 5b) and precipitation (Fig. 6) because snow turns into rain only when it falls to the melting layer. Moreover, since the cloud water and ice cannot coexist in the WSM3 CM scheme, the accretion of cloud ice by snow is less efficient. That may be a major reason for the smaller amount of snow produced in WSM3 than in WSM5 (Figs. 8d and 5d). Accordingly, WSM3 produces the weakest convective heating rate among all experiments with the maximum value of 10 K h^{-1} , which is less than 1/2 of the maximum value in KS (Fig. 9c).

In the WSM5 CM scheme, the mixed phase of hydrometeors is allowed. The melting and freezing processes occur in a deeper layer than in WSM3 (Hong and Lim 2006). The autoconversion from cloud to rain is also more efficient. As a result, WSM5 produces larger amounts of rainwater and precipitation (Figs. 8b and 6) than WSM3. In addition, the more efficient accretion of cloud and ice by snow due to the existence of the mixed phase of hydrometeors causes a larger amount of snow formed in WSM5 than WSM3 (Figs. 8d and 5d). Accordingly, the convective heating rate in WSM5 is much stronger than that in WSM3 (Fig. 9d). Comparing with WSM6 and LIN, WSM5 produces smaller amount of precipitation (Fig. 6) and larger amount of total water loading (Figs. 5f and 8f). This may be attributed to the exclusion of graupel in WSM5. With no graupel, the only precipitating ice in WSM5 is snow. As snow has a smaller fall velocity than graupel, the precipitation rate in WSM5 is smaller than in WSM6.

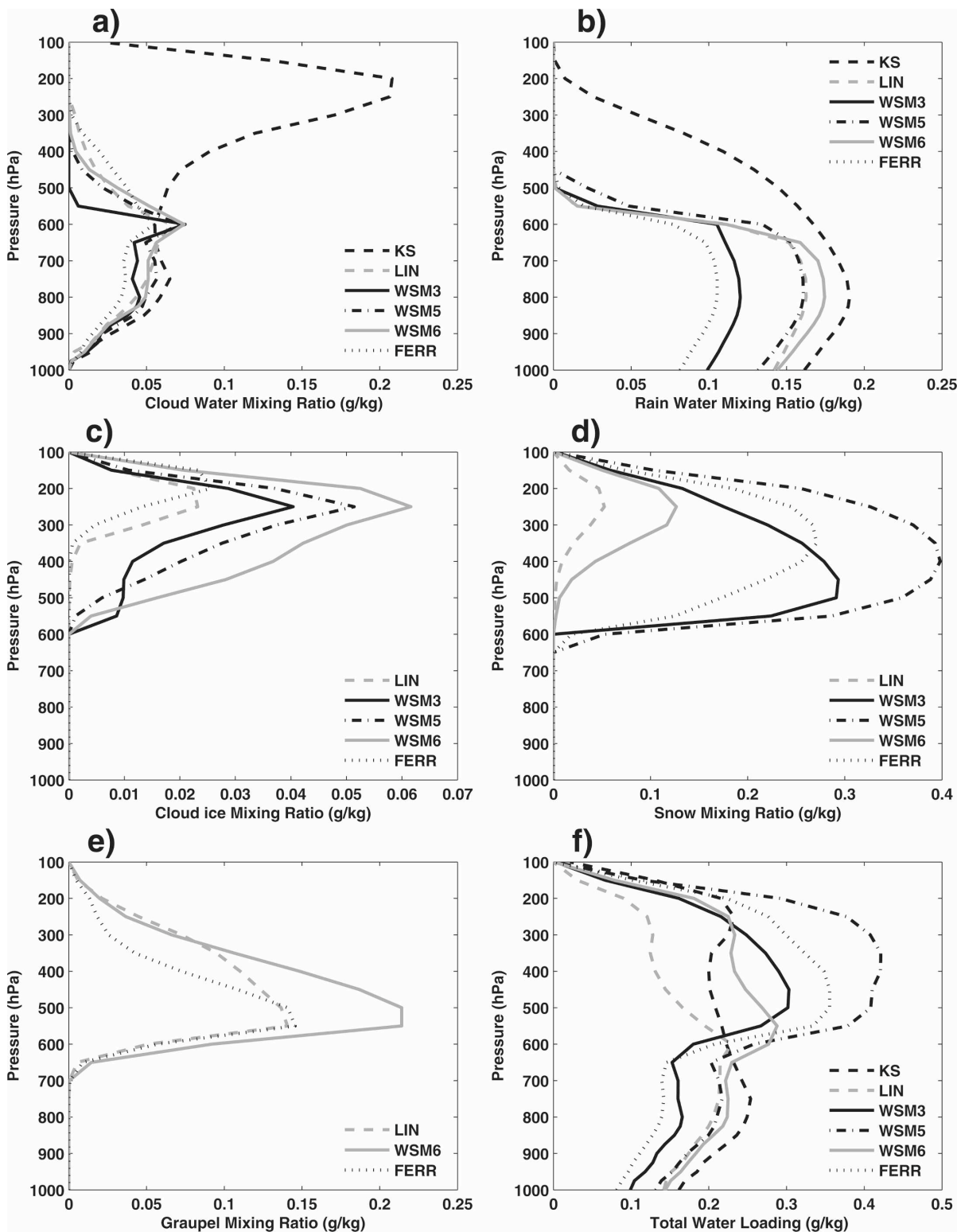


FIG. 8. Vertical distributions of area-averaged (g kg^{-1} ; within the 250-km radius from the storm center) (a) cloud water, (b) rainwater, (c) cloud ice, (d) snow, (e) graupel, and (f) total water loading at 0600 UTC 15 Jul 2005.

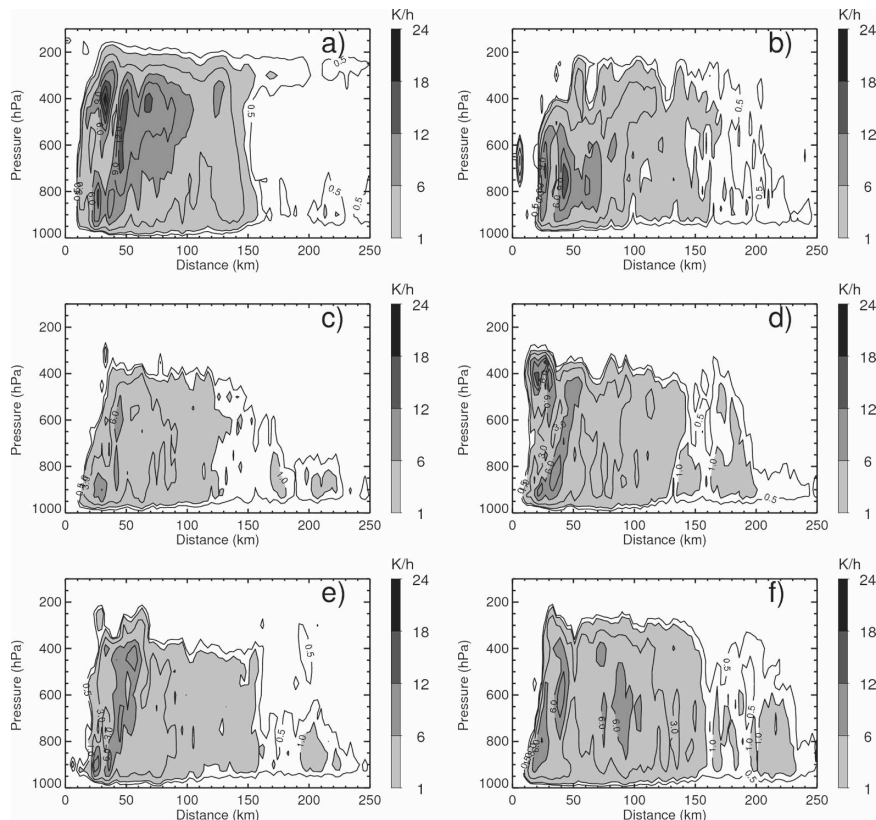


FIG. 9. Radius–height distribution of convective heating rate at 0600 UTC 15 Jul 2005 for experiments (a) KS, (b) LIN, (c) WSM3, (d) WSM5, (e) WSM6, and (f) FERR.

Notable differences in hydrometeor distributions are produced among LIN, WSM6, and FERR, although they are all six-class ice-phase CM schemes. When compared with LIN and FERR, WSM6 produces larger amounts of rainwater, cloud ice, and graupel (Figs. 5 and 8). The fallouts of rainwater and graupel yield a high precipitation rate in WSM6 (Fig. 6). In the other two experiments, LIN produces larger amounts of cloud water, rainwater, and graupel, and smaller amounts of snow than FERR does (Fig. 8). It could be a major reason for the stronger rainfall in LIN than in FERR. FERR, however, produces the smallest amount of cloud and rainwater at the mid- to low troposphere among all experiments (Figs. 8a,b). In addition, FERR also generates more snow and less graupel than both WSM6 and LIN (Figs. 8d,e). These factors result in the smallest amount of precipitation produced by FERR among all experiments. Corresponding to the different hydrometeors distributions, the latent heats in the three experiments display quite different structures. Specifically, LIN produces the maximum in convective heating near 700 hPa (Fig. 9b) as a result of the larger formation of the hydrometeors aloft (Fig. 8f). The peak in convective heating, located at 400 hPa (Fig. 9e) in WSM6,

mainly reflects the large amount of graupel in the mid- to high troposphere (Fig. 8e). The FERR, on the other hand, shows maximum convective heating at about the 600-hPa pressure level (Fig. 9f), mainly related to the formation of snow and graupel in the mid- to high troposphere.

b. Inner-core convective and thermal structure

Figure 10 shows the southwest–northeast cross section of vertical velocity through the storm center at 0600 UTC 15 July 2005. Corresponding to the strong eyewall convective heating (Fig. 9a), KS produces a strong eyewall updraft, which penetrates up to 150–100 hPa (Fig. 10a). This may be a realistic updraft structure, but it is apparently *not* being produced for correct reasons. The weakest eyewall convection produced by WSM3 among all experiments (Fig. 10c) agrees well with the weak convective heating (Fig. 9c). The eyewall updraft is much stronger in WSM5 than in WSM3 (Fig. 10d), which corresponds to the stronger latent heat release (Fig. 9d). When compared with FERR, LIN produces a stronger eyewall convection (Fig. 10b), mainly reflecting the larger heating rate over storm eyewall (Fig. 9b).

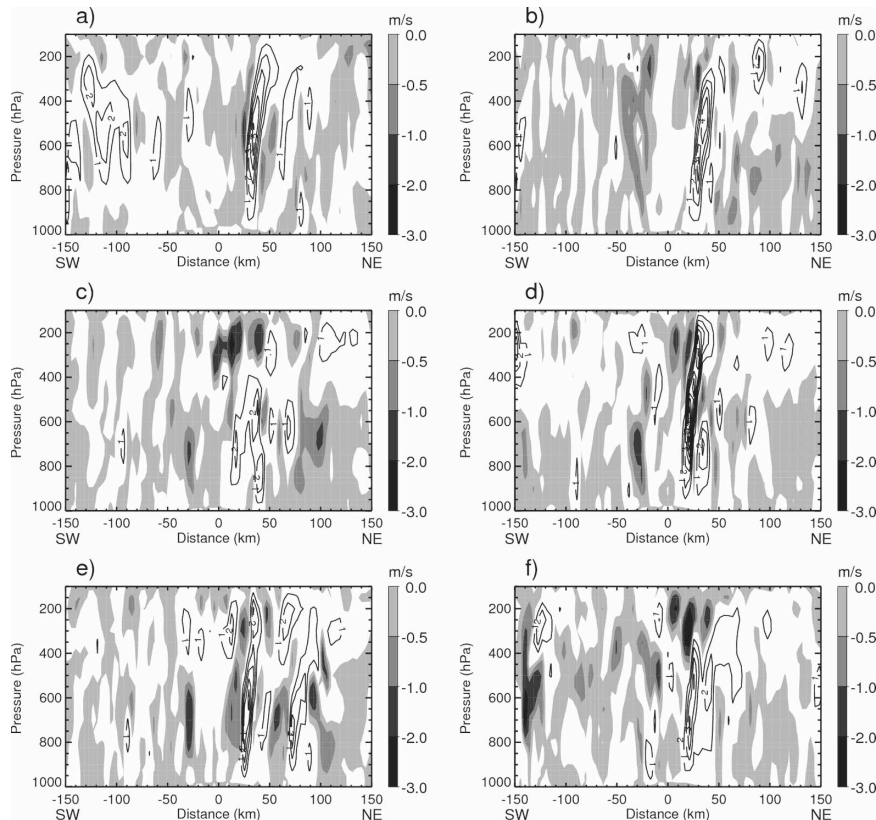


FIG. 10. Southwest–northeast cross sections of the vertical velocity (m s^{-1}) through the storm center at 0600 UTC 15 Jul 2005: (a) KS, (b) LIN, (c) WSM3, (d) WSM5, (e) WSM6, and (f) FERR. The shaded contour presents the negative value of vertical velocity (downdraft) and the line contour denotes the positive value of vertical velocity (updraft).

The heating caused by the descending motion in the storm eye usually contributes to the formation of the hurricane warm core. The warming over the core region can represent the hurricane center pressure (Willoughby 1995). To illustrate more about the differences in the simulated storm structure, Fig. 11 shows the southwest–northeast cross section through the storm center for temperature anomaly, calculated by removing the average value at each pressure levels from the temperature field, at 0600 UTC 15 July 2005. The strongest warm center is produced by KS with the maximum temperature anomaly of over 10°C (Fig. 11a). The weakest warm center (with a temperature anomaly of 6°C ; Fig. 11c) is produced by WSM3, which corresponds to the weakest storm produced in this experiment. Compared with WSM3, stronger warm cores are formed in LIN, WSM5, and WSM6 with the extreme temperature anomalies of $\sim 7^{\circ}\text{--}8^{\circ}\text{C}$ (Figs. 11b,d,e), which correspond well to the deeper storm intensities in these experiments.

Figure 11 shows that most warm cores are located between the 500- and 400-hPa pressure levels. This po-

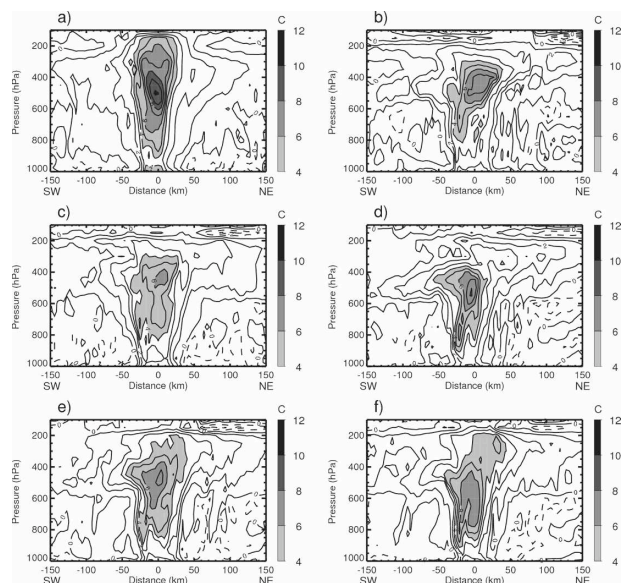


FIG. 11. As in Fig. 10 but for temperature anomaly ($^{\circ}\text{C}$).

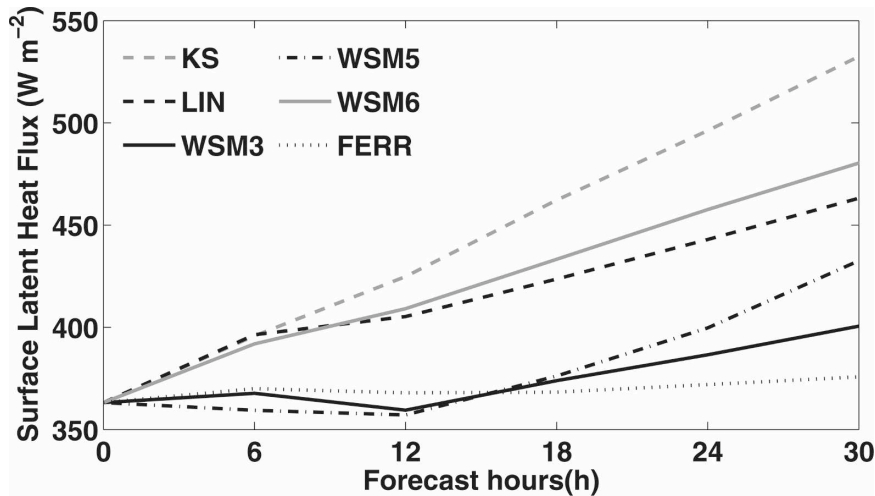


FIG. 12. Time series (6-h interval) of the area-averaged (within the 250-km radius from the storm center) latent heat flux (W m^{-2}) during 0600 UTC 14 Jul–1200 UTC 15 Jul 2005.

sition is much lower than that documented in Hawkins and Rubsam (1968), in which the warm core of Hurricane Hilda (1964) is located around 250 hPa with a maximum temperature anomaly of 16°C and MSLP of 940 hPa. Another study by Hawkins and Imbembro (1976) showed that Hurricane Inez (1966) has its warm core observed between the 350- and 250-hPa pressure levels with the maximum temperature anomaly of 9°C and MSLP of about 960 hPa. Compared with the structures of these two intense hurricanes, it seems that the vertical locations of the simulated warm cores of Hurricane Emily are too low. Even in KS, the maximum temperature anomaly is over 10°C , but the warm-core center is still located between 600 and 400 hPa. The lower warm-core positions may be attributed to the lack of the narrow cyclonic circulation at the upper level to tropopause in the numerical simulations (Fig. 10).

c. Surface energy transport

The ocean surface has long been recognized as an important factor in the development of hurricanes (Byers 1944). Davis and Emanuel (1988) showed that TC intensification depends greatly on the sensible and latent heat flux from the ocean surface. Emanuel (1986, 1993) suggested the Wind Induced Surface Heat Exchange (WISHE) is an important factor in TC development. They demonstrated that TCs can be maintained solely by the latent and sensible heat fluxes that are drawn from the ocean surface without any support from ambient conditional instability. To investigate the impact of surface heat flux on Hurricane Emily's development, Fig. 12 compares the time series (i.e., the

6-h interval) of surface latent heat flux averaged over the storm core region (within the 250-km radius from the storm center) in different experiments during 0600 UTC 14 July–1200 UTC 15 July 2005. The figure indicates that the intensity of the simulated storm is well correlated to the mean surface latent heat flux. Specifically, the largest magnitude and the most rapidly increasing rate of surface latent heat flux corresponds to the most intense storm with the most rapid intensification rate in KS. Meanwhile, the weak storm produced in WSM3, corresponds to the low magnitude with small changes in the mean surface latent heat flux.

The equivalent potential temperature θ_e commonly increases toward the center in a TC. Previous studies showed that high θ_e air feeding from the ocean surface is an important mechanism for the maintenance and development of hurricane eyewall convection (Willoughby 1995; Chen and Yau 2003). The sensible and latent heat flux from the ocean surface is one of the more important causes of θ_e increase in the eyewalls of hurricanes. Liu et al. (1999) showed that the surface latent heat flux accounts for 64% of the increase of θ_e from a radius of 150 km to the eye of hurricane. To demonstrate further the impact of ocean surface on the structure of the simulated storms, Fig. 13 compares the radius–height distribution of θ_e from all experiments at 0600 UTC 15 July 2005. It is found that the maxima θ_e have a good correlation with the simulated maximum storm intensity and the magnitude of the mean surface latent heat flux. In KS, the maximum θ_e at the storm center is 378 K. It is much larger than that in other experiments. In contrast, WSM3 produces a maximum θ_e of 363 K, which is 15 K lower than in KS. When

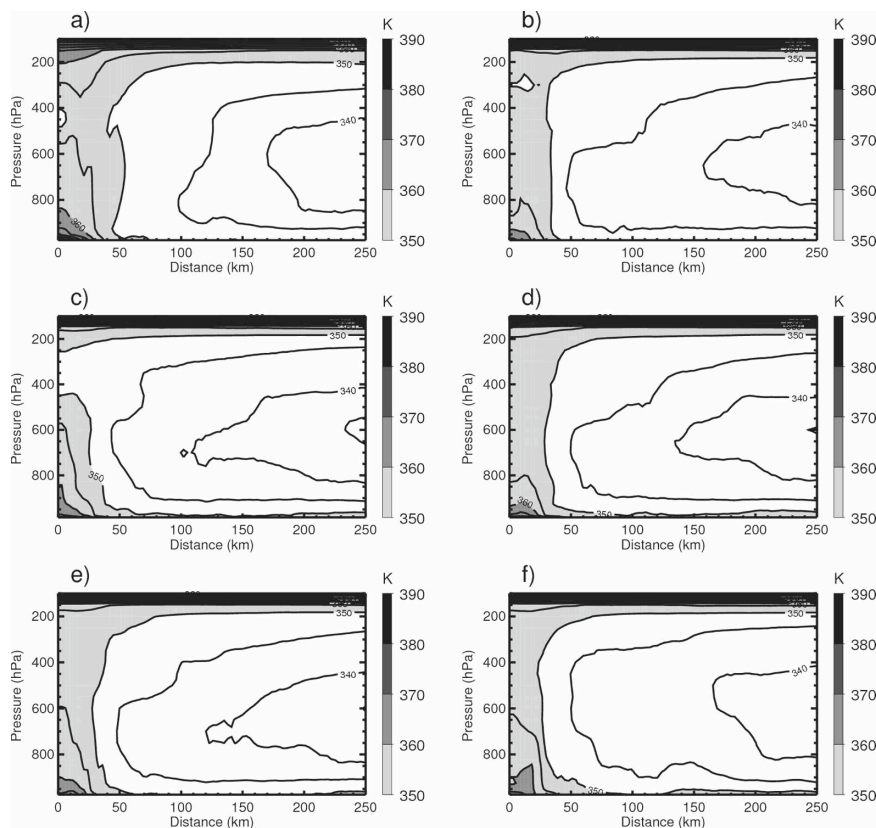


FIG. 13. As in Fig. 9 but for θ_e (K).

compared with WSM3, other schemes such as WSM5, WSM6, FERR, and LIN produce higher surface θ_e . Overall, the results indicate that the latent heat flux and high θ_e air feeding from the ocean surface are very important factors influencing the simulated intensities of Hurricane Emily. Another interesting feature in Fig. 13 is that the change in surface θ_e extends to a quite large area in both WSM5 and FERR. Considering the large amount of high θ_e appeared in the two experiments, it appears that these two schemes tend to release the instability energy more rapidly.

As the above results indicated, the differences in the energy flux from the ocean surface make an important contribution to the different intensification procedures in various experiments. Specifically, the larger energy and moisture absorption from the ocean surface (Figs. 12 and 13a), together with the stronger latent heat release (Fig. 9) and the absence of the cooling due to exclusion of the melting processes in this scheme, results in more intense eyewall convection (Fig. 10a) with a stronger lower-level convergence and upper-level divergence (Fig. 14a); hence, a more rapid development is produced in KS (Fig. 4). In contrast, WSM3 has a smaller amount of heat and moisture fluxes from the

ocean surface (Figs. 12 and 13c) into the eyewall, and a weaker eyewall latent heat release (Fig. 9c). Because of these features, a weaker eyewall convection (Fig. 10c), and a weaker low-level convergence and upper-level divergence (Fig. 14c) are produced. As a result, the slowest intensification rate is produced in WSM3 (Fig. 4).

d. 850–200-hPa environmental vertical wind shear

Environmental vertical wind shear is another important factor that could influence hurricane structure and development. Merrill (1988) and Frank and Ritchie (1999) concluded that weak environmental vertical wind shear is a necessary condition for TC deepening; however, the impact of environmental vertical wind shear on hurricane development during the rapid intensification period is still unclear (Zehr 2003). Paterson et al. (2005) suggested that the most favorable wind shear for the rapid intensification of a tropical storm is about $\sim 2\text{--}4\text{ m s}^{-1}$, while Black et al. (2002) found that Hurricane Olivia (1994) intensified remarkably with a vertical wind shear of 8 m s^{-1} . The inconsistency in these results suggests the need to further examine the influence of vertical wind shear on TC rapid intensification.

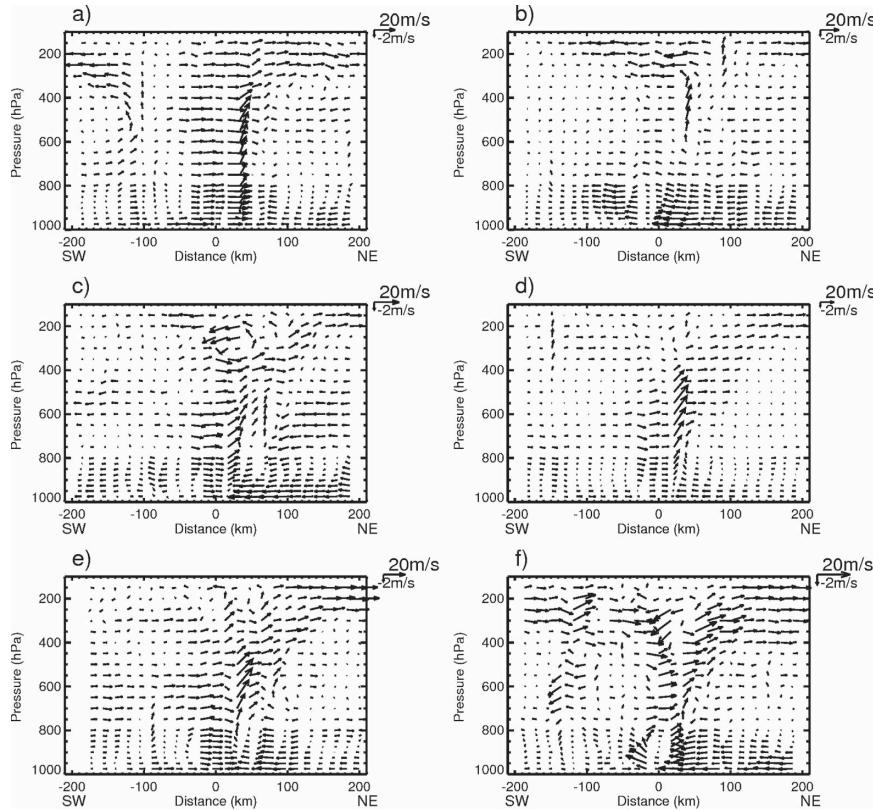


FIG. 14. As in Fig. 10 but of the wind vector (m s^{-1} ; storm relative horizontal wind and vertical velocity).

Figure 15 illustrates the time series of the environmental vertical shear calculated from the difference between 850 and 200 hPa wind vectors averaged in the area between the 200- and 800-km radius from the storm center, following Braun et al. (2006) and Kaplan and DeMaria (2003). The magnitudes of vertical wind shear are less than 8 m s^{-1} in all experiments except FERR, which produced much stronger vertical wind shear than all other experiments during the whole simulation period. The vertical wind shear in KS is less than 6 m s^{-1} in the first 12 h of the simulation and then increases slowly to 7 m s^{-1} as the storm intensifies very rapidly from a category 1 to a category 3 hurricane, whereas the vertical wind shear in LIN increases slowly from 5.5 to 6 m s^{-1} in the first 12 h before it decreases from 6 to 4.9 m s^{-1} in the next 18 h. Hence, the magnitude of the vertical wind shear in LIN is 2.1 m s^{-1} lower than that in KS when the MSLP in LIN is 18 hPa higher than in KS at 1200 UTC 15 July. In addition, WSM3, WSM5, and WSM6 all produce similar trends in the change of the vertical wind shear with the maximum difference of 1.2 m s^{-1} . Based on these results, *the magnitudes of vertical wind shear do not correspond well to the simulated intensities of Hurricane Emily*. This

conclusion obviously contradicts the typical view on the relationship between vertical wind shear and TC deepening, and may be case dependent. However, Zhu et al. (2004) showed that Hurricane Bonnie (1998) intensified rapidly from 974 hPa at 0600 UTC 23 August to 952 hPa at 0000 UTC 24 August 1998 with the vertical

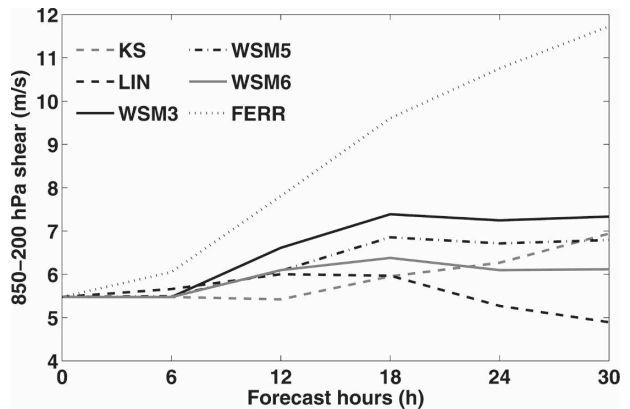


FIG. 15. Time series (6-h interval) of vertical wind shear (m s^{-1}) between 200 and 850 hPa averaged over the area between the 200- and 800-km radius from the storm center during 0600 UTC 14 Jul–1200 UTC 15 Jul 2005.

TABLE 4. List of the PBL sensitivity experiments and their physics options.

Expt	Cloud microphysics scheme	PBL scheme
WSM3	WSM three-class simple ice	YSU
WSM6	WSM six-class graupel	YSU
WSM3 + MYJ	WSM three-class simple ice	MYJ
WSM6 + MYJ	WSM six-class graupel	MYJ

wind shear increasing from 10 to 18 m s^{-1} . They suggested that the relationship between vertical wind shear and TC intensification is more complicated than previously thought. Therefore, more studies are needed to further investigate the effect of vertical wind shear during rapid hurricane intensification.

5. Sensitivity to PBL schemes and model resolution

a. Sensitivity to PBL schemes

The above results show that the energy flux from the ocean surface is an important factor influencing the simulated intensity of Hurricane Emily. To further examine this issue, additional set of experiments are conducted using different combinations of PBL and CM schemes, the YSU PBL scheme and the Mellor–Yamada–Janjic (MYJ) PBL scheme and the WSM3 and WSM6 CM schemes. The corresponding physics options for these experiments are listed in Table 4. All experiments use the same model domains, initial conditions, and boundary conditions as described in section 3.

The YSU and MYJ PBL schemes differ in their ways of calculating the surface fluxes and the vertical mixing in the PBL. The YSU PBL scheme (Hong et al. 2006) is the new version of the Medium-Range Forecast (MRF) PBL scheme (Hong and Pan 1996). It is a “nonlocal K ” scheme. This approach uses the countergradient fluxes to determine the depth of the PBL, and then constrains the vertical diffusion coefficient to a fixed profile within the PBL. The YSU scheme improves the MRF scheme by including an explicit treatment of entrainment process at the top of the PBL, which can help to avoid the excessive mixing in the mixed layer during strong wind events. The MYJ scheme, however, is a “local K ” scheme (Janjic 2002). The diffusivity coefficients are parameterized as functions of the local Richardson number. The Mellor–Yamada level 2.5 turbulence closure model, which includes a prognostic equation for the turbulent kinetic energy, is used in this scheme. The height of the PBL is estimated from the TKE production. The nonsingularity constraint for the TKE production is used under unstable atmosphere conditions.

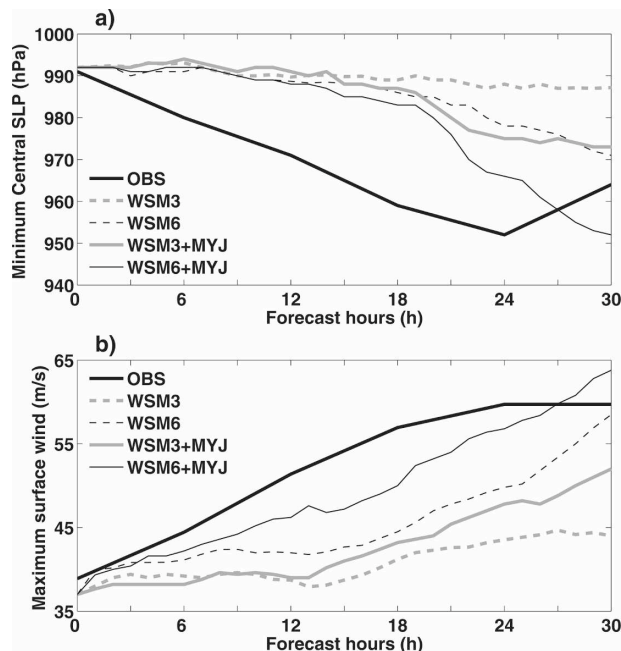


FIG. 16. As in Fig. 4, but for the PBL sensitivity experiments during 0600 UTC 14 Jul–1200 UTC 15 Jul 2005.

Figure 16 shows the intensity forecasts from all experiments. It is apparent that the intensity forecast is sensitive to the PBL schemes in the ARW model. At the end of the simulations, the forecast storm intensities vary from a 12-hPa (9 m s^{-1}) overdeepening to a 20-hPa (16 m s^{-1}) underdeepening in MSLP (MSW). The strongest storm is produced by WSM6 + MYJ, and the weakest storm is produced by WSM3 + YSU. Overall, with different PBL schemes, the simulated MSLP varies by 19 hPa. When compared with the YSU PBL scheme, the MYJ scheme produces stronger storms. In addition, the result also shows that the interaction between the physical processes in the numerical model can be very important. Specifically, when the MYJ PBL scheme is used, the simulation with WSM3 CM scheme produces a similar storm intensity to that of the experiment with the WSM6 CM and YSU PBL schemes. This result highlights the need for caution when choosing the model’s physical parameterizations in numerical simulations.

To illustrate the factors that cause the stronger storms generated by the simulations with the MYJ PBL scheme, Fig. 17 shows the time series (i.e., the 6-h interval) of surface latent heat flux averaged within the 250-km radius from the storm center. The result illustrates a close correlation between the simulated intensity changes and the magnitudes of the mean surface latent heat flux. The simulations with the MYJ PBL scheme produce a stronger surface latent heat flux than

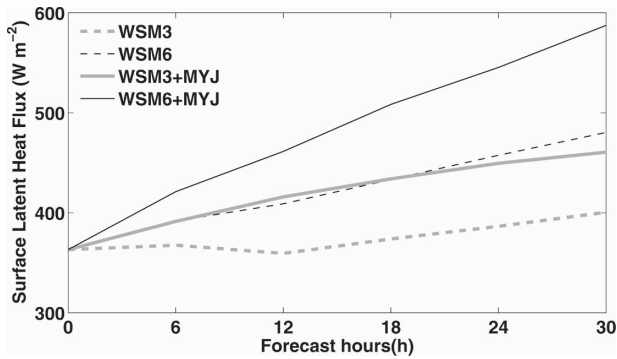


FIG. 17. As in Fig. 12, but for the PBL sensitivity experiments.

those with the YSU PBL scheme. In particular, the largest value and the most rapidly increasing rate of surface latent heat flux lead to the most intense storm and the most rapid intensification rate by WSM6 + MYJ. In WSM3 + YSU, the mean surface latent heat flux has the smallest value in the whole simulation period and results in the weakest storm among all experiments. The differences in surface heat flux and storm intensity among the simulations can be attributed to the different features of the YSU and MYJ PBL schemes. According to Braun and Tao (2000), the nonlocal scheme tends to have stronger warming and drying at the low level of the PBL. This strong warming and drying result from the larger value of the eddy exchange coefficient that exists in a deeper layer. The drying of the lower PBL causes a higher cloud base and smaller heat and moisture fluxes from the ocean surface. The weaker storm intensity in simulations with the YSU PBL scheme is closely related to these features in PBL. The local- K MYJ scheme does not transport the moisture and heat away from the surface as deeply and strongly as the nonlocal YSU scheme (Holtslag and Boville 1993). Therefore, the MYJ scheme produces a greater moistening in the PBL, lower cloud base, and larger surface water and heat fluxes. This explains the deeper storms produced by experiments with the MYJ PBL scheme.

b. Impact of the model horizontal resolution

It is believed that hurricane intensity forecasts can be improved by adopting higher model grid resolution. Davis et al. (2006) showed that the forecasts of land-falling Atlantic TCs in 2004 and 2005 have been significantly improved by increasing the model horizontal grid spacing from 12 to 4 km. Further increasing of the model horizontal resolution to 1.33 km in the simulation of Hurricane Katrina was able to intensify the storm more rapidly.

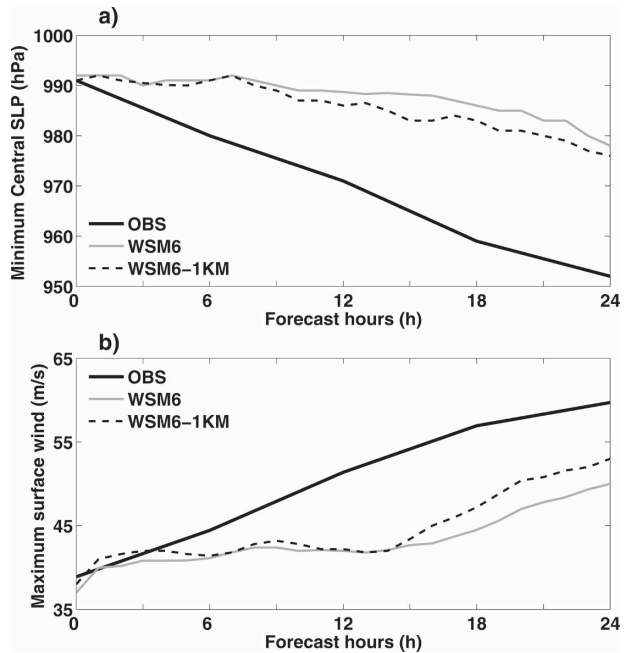


FIG. 18. As in Fig. 4, but for experiments with different model horizontal resolutions during 0600 UTC 14 Jul–0600 UTC 15 Jul 2005.

In this study the ARW model fails to predict the rapid intensification of Hurricane Emily at 3-km horizontal resolution. An additional attempt is made with the model grid spacing of 1 km to examine whether this higher resolution would help improve the forecasts of rapid intensification. A 1-km grid domain is then nested into the 3-km grids domain in the WSM6 experiment (domain location not shown). The result (Fig. 18) indicates that increasing the model horizontal resolution is helpful but only results in a marginal improvement. At the end of the simulation, the simulated MSLP is only 3 hPa deeper than that produced by the simulation at 3-km resolution. In other words, resolution alone does not compensate for other shortcomings of the simulation.

6. Concluding remarks

A series of numerical simulations is conducted with the ARW model to examine the sensitivity of short-range numerical simulations of Hurricane Emily's (2005) early rapid intensification to the CM and PBL parameterizations, and model horizontal resolutions. The results show that the numerical simulation of Emily's early rapid intensification is very sensitive to the choice of various CM and PBL parameterization schemes. Although all of the simulations start from the same initial intensity, the simulated storm intensities

vary by up to 29 hPa with the use of six different CM schemes in a 30-h simulation period. Even if the two extreme cases with simple KS and WSM3 CM schemes were not taken into account, the difference in the simulated MSLP, produced by these relatively advanced CM schemes (such as the FERR, LIN, WSM5, and WMS6), still varies by up to 10 hPa. In addition, the boundary layer processes also have a significant influence on the simulated hurricane intensity. Two different PBL schemes (YSU and MYJ) result in a difference in the simulated MSLP by up to 19 hPa.

Physical and dynamic processes associated with the sensitivities are investigated. It is found that the strength of the environmental vertical wind shear is not well correlated with the simulated hurricane intensities, implying that the vertical wind shear does not exert a simple effect on the simulated intensity changes during the rapid intensification of Hurricane Emily. In contrast, the storm internal structure has been greatly influenced by various CM and PBL schemes. Structures of eyewall convective heating distributions, surface latent heat flux, and low-level θ_e are quite different in the various experiments. The simulations of storm intensity are closely related with these differences. Specifically, stronger latent heat release, larger ocean surface energy flux, and higher low-level θ_e are evident in the more enhanced convection and intense storms.

The CM schemes used in this study differ in their complexity and hydrometeor species. Although the Kessler scheme has resulted in the most rapid intensification rate and the “best” forecast of Emily’s intensity because of the reason addressed above, it does not mean that KS is a scheme one should choose in future simulations. The results from this study indicate the reason why different CM and PBL schemes result in different intensity forecasts and the physical processes that contribute to storm intensification. It is also suggested that contributions from the CM and PBL processes in the ARW model can only partially explain the slow intensification rate of Hurricane Emily produced by the ARW model.

In this study, the ARW model fails to predict Emily’s rapid intensification with a 3-km horizontal resolution. However, increasing the model horizontal resolution to 1 km is somewhat helpful, but it still does not result in a good forecast, since most of above conclusions are based on one case study; thus, more work is needed in order to draw more general conclusions. In addition, more investigation is certainly necessary in order to fully understand the reasons for shortcomings in hurricane intensity forecasts. For instance, since our study showed the importance of the energy transport from the ocean surface, the deficiencies in Emily’s intensity

change forecast may also be partly related to the lack of air–ocean interactions. More studies are proposed as future work.

Acknowledgments. The authors acknowledge the WRF Model working group for their efforts to develop a mesoscale community model. They are also very grateful to Dr. Edward Zipser at the University of Utah and three anonymous reviewers for their valuable comments that helped to improve the manuscript. This study is supported by the NASA TCSP (Grant NNG05GH82G) and EOS Programs (Grant NNX08AD32G). Computer time was provided by the Center for High Performance Computing (CHPC) at the University of Utah.

REFERENCES

- Anthes, R. A., and S. W. Chang, 1978: Response of the hurricane boundary layer to changes of sea surface temperature in a numerical model. *J. Atmos. Sci.*, **35**, 1240–1255.
- Barker, D. M., W. Huang, Y. R. Guo, and Q. N. Xiao, 2004: A three-dimensional (3DVAR) data assimilation system for use with MM5: Implementation and initial results. *Mon. Wea. Rev.*, **132**, 897–914.
- Bender, M. A., and I. Ginis, 2000: Real-case simulations of hurricane–ocean interaction using a high-resolution coupled model: Effects on hurricane intensity. *Mon. Wea. Rev.*, **128**, 917–946.
- Black, M. L., J. F. Gamache, F. D. Marks Jr., C. E. Samsury, and H. E. Willoughby, 2002: Eastern Pacific Hurricanes Jimena of 1991 and Olivia of 1994: The effect of vertical shear on structure and intensity. *Mon. Wea. Rev.*, **130**, 2291–2312.
- Bosart, L. F., C. S. Velden, W. E. Bracken, J. Molinari, and P. G. Black, 2000: Environmental influences on the rapid intensification of Hurricane Opal (1995) over the Gulf of Mexico. *Mon. Wea. Rev.*, **128**, 322–352.
- Braun, S. A., and W.-K. Tao, 2000: Sensitivity of high-resolution simulations of Hurricane Bob (1991) to planetary boundary layer parameterizations. *Mon. Wea. Rev.*, **128**, 3941–3961.
- , M. T. Montgomery, and Z. Pu, 2006: High-resolution simulation of Hurricane Bonnie (1998). Part I: The organization of eyewall vertical motion. *J. Atmos. Sci.*, **63**, 19–42.
- Byers, H. R., 1944: *General Meteorology*. McGraw-Hill, 645 pp.
- Chen, S.-H., and W.-Y. Sun, 2002: A one-dimensional time-dependent cloud model. *J. Meteor. Soc. Japan*, **80**, 99–118.
- Chen, Y., and M. K. Yau, 2003: Asymmetric structure in a simulated landfalling hurricane. *J. Atmos. Sci.*, **60**, 2294–2312.
- Davis, C. A., and K. A. Emanuel, 1988: Observational evidence for the influence of surface heat fluxes on rapid maritime cyclogenesis. *Mon. Wea. Rev.*, **116**, 2649–2659.
- , and L. F. Bosart, 2002: Numerical simulations of the genesis of Hurricane Diana. Part II: Sensitivity of track and intensity prediction. *Mon. Wea. Rev.*, **130**, 1100–1124.
- , and Coauthors, 2006: Advanced research WRF developments for hurricane prediction. *Seventh WRF Users’ Workshop*, Boulder, CO, National Center for Atmospheric Research, 3.1. [Available online at <http://www.mmm.ucar.edu/wrf/users/workshops/WS2006/WorkshopPapers.htm>.]
- De Maria, M., and J. D. Pickle, 1988: A simplified system of equa-

- tions for simulation of tropical cyclones. *J. Atmos. Sci.*, **45**, 1542–1554.
- Dudhia, J., 1989: Numerical study of convection observed during the winter monsoon experiment using a mesoscale two-dimensional model. *J. Atmos. Sci.*, **46**, 3077–3107.
- Emanuel, K. A., 1986: An air–sea interaction theory for tropical cyclones. Part I: Steady-state maintenance. *J. Atmos. Sci.*, **43**, 585–604.
- , 1993: The effect of convective response time on WISHE modes. *J. Atmos. Sci.*, **50**, 1763–1776.
- Frank, W. M., 1977: The structure and energetics of the tropical cyclone. II: Dynamics and energetics. *Mon. Wea. Rev.*, **105**, 1136–1150.
- , and E. A. Ritchie, 1999: Effects of environmental flow upon tropical cyclone structure. *Mon. Wea. Rev.*, **127**, 2044–2061.
- Franklin, J. L., and D. P. Brown, cited 2006: Tropical cyclone report: Hurricane Emily, 11–21 July 2005. National Hurricane Center Report. [Available online at http://www.nhc.noaa.gov/pdf/TCR-AL052005_Emily.pdf.]
- Grabowski, W. W., 1998: Toward cloud resolving modeling of large-scale tropical circulations: A simple cloud microphysics parameterization. *J. Atmos. Sci.*, **55**, 3283–3298.
- Grell, G. A., and D. Dévényi, 2002: A generalized approach to parameterizing convection combining ensemble and data assimilation techniques. *Geophys. Res. Lett.*, **29**, 1693, doi:10.1029/2002GL015311.
- Halverson, J. B., and Coauthors, 2007: NASA's Tropical Cloud Systems and Processes (TCSP) experiment. *Bull. Amer. Meteor. Soc.*, **88**, 867–882.
- Hawkins, H. F., and D. T. Rubsam, 1968: Hurricane Hilda, 1964. *Mon. Wea. Rev.*, **96**, 701–707.
- , and S. M. Imbembo, 1976: The structure of a small, intense hurricane—Inez 1966. *Mon. Wea. Rev.*, **104**, 418–442.
- Holtstlag, A. A. M., and B. A. Boville, 1993: Local versus nonlocal boundary layer diffusion in a global climate model. *J. Climate*, **6**, 1825–1842.
- Hong, S.-Y., and H.-L. Pan, 1996: Nonlocal boundary layer vertical diffusion in a medium-range forecast model. *Mon. Wea. Rev.*, **124**, 2322–2339.
- , and J.-O. Lim, 2006: The WRF single-moment 6-class microphysics scheme (WSM6). *J. Korean Meteor. Soc.*, **42**, 129–151.
- , J. Dudhia, and S.-H. Chen, 2004: A revised approach to ice microphysical processes for the bulk parameterization of clouds and precipitation. *Mon. Wea. Rev.*, **132**, 103–120.
- , Y. Noh, and J. Dudhia, 2006: A new vertical diffusion package with an explicit treatment of entrainment processes. *Mon. Wea. Rev.*, **134**, 2318–2341.
- Houze, R. A., Jr., and Coauthors, 2006: The Hurricane Rainband and Intensity Change Experiment: Observations and modeling of Hurricanes Katrina, Ophelia, and Rita. *Bull. Amer. Meteor. Soc.*, **87**, 1503–1521.
- Huffman, G. J., and Coauthors, 2007: The TRMM Multisatellite Precipitation Analysis (TMPA): Quasi-global, multiyear, combined-sensor precipitation estimates at fine scales. *J. Hydrometeorol.*, **8**, 38–55.
- Janjic, Z. I., 2002: Nonsingular implementation of the Mellor–Yamada level 2.5 scheme in the NCEP global model. NCEP Office Note 437, 61 pp. [Available at NCEP/EMC, 5200 Auth Road, Camp Springs, MD 20746.]
- Kaplan, J., and M. DeMaria, 2003: Large-scale characteristics of rapidly intensifying tropical cyclones in the North Atlantic basin. *Wea. Forecasting*, **18**, 1093–1108.
- Karyampudi, V. M., G. S. Lai, and J. Manobianco, 1998: Impact of initial conditions, rainfall assimilation, and cumulus parameterization on simulations of Hurricane Florence (1988). *Mon. Wea. Rev.*, **126**, 3077–3101.
- Kessler, E., 1969: *On the Distribution and Continuity of Water Substance in Atmospheric Circulation*. Meteor. Monogr., No. 32, Amer. Meteor. Soc., 84 pp.
- Krishnamurti, T. N., S. Pattnaik, L. Stefanova, T. S. V. Vijaya Kumar, B. P. Mackey, A. J. O'Shay, and R. J. Pasch, 2005: The hurricane intensity issue. *Mon. Wea. Rev.*, **133**, 1886–1912.
- Kuo, Y.-H., M. A. Shapiro, and E. G. Donall, 1991: The interaction between baroclinic and diabatic processes in a numerical simulation of a rapidly intensifying extratropical marine cyclone. *Mon. Wea. Rev.*, **119**, 368–384.
- Li, X., and Z. Pu, 2006: Sensitivity of numerical simulations of Hurricane Emily (2005) to cumulus and microphysical parameterizations in the WRF model. Preprints, *27th Conf. on Hurricanes and Tropical Meteorology*, Monterey, CA, Amer. Meteor. Soc., 16A.1. [Available online at <http://ams.confex.com/ams/pdfpapers/108959.pdf>.]
- Lin, Y.-L., R. D. Farley, and H. D. Orville, 1983: Bulk parameterization of the snow field in a cloud model. *J. Climate Appl. Meteor.*, **22**, 1065–1092.
- Liu, Y., D.-L. Zhang, and M. K. Yau, 1999: A multiscale numerical study of Hurricane Andrew (1992). Part II: Kinematics and inner-core structures. *Mon. Wea. Rev.*, **127**, 2597–2616.
- Lord, S. J., and J. M. Lord, 1988: Vertical velocity structures in an axisymmetric, nonhydrostatic tropical cyclone model. *J. Atmos. Sci.*, **45**, 1453–1461.
- , H. E. Willoughby, and J. M. Piotrowicz, 1984: Role of a parameterized ice-phase microphysics in an axisymmetric, nonhydrostatic tropical cyclone model. *J. Atmos. Sci.*, **41**, 2836–2848.
- Malkus, J. S., 1958: On the structure and maintenance of the mature hurricane eye. *J. Meteor.*, **15**, 337–349.
- McFarquhar, G. M., H. Zhang, G. Heymsfield, R. Hood, J. Dudhia, J. B. Halverson, and F. Marks Jr., 2006: Factors affecting the evolution of Hurricane Erin (2001) and the distributions of hydrometeors: Role of microphysical processes. *J. Atmos. Sci.*, **63**, 127–150.
- Merrill, R. T., 1988: Environmental influences on hurricane intensification. *J. Atmos. Sci.*, **45**, 1678–1687.
- , and C. S. Velden, 1996: A three-dimensional analysis of the outflow layer of Supertyphoon Flo (1990). *Mon. Wea. Rev.*, **124**, 47–63.
- Mlawer, E. J., S. J. Taubman, P. D. Brown, M. J. Iacono, and S. A. Clough, 1997: Radiative transfer for inhomogeneous atmosphere: RRTM, a validated correlated-k model for the longwave. *J. Geophys. Res.*, **102** (D14), 16 663–16 682.
- Montgomery, M. T., M. M. Bell, S. D. Aberson, and M. L. Black, 2006: Hurricane Isabel (2003): New insights into the physics of intense storms. Part I: Mean vortex structure and maximum intensity estimates. *Bull. Amer. Meteor. Soc.*, **87**, 1335–1347.
- Park, K., and X. Zou, 2004: Toward developing an objective 4DVAR BDA scheme for hurricane initialization based on TPC observed parameters. *Mon. Wea. Rev.*, **132**, 2054–2069.
- Paterson, L. A., B. N. Hanstrum, N. E. Davidson, and H. C. Weber, 2005: Influence of environmental vertical wind shear on the intensity of hurricane-strength tropical cyclones in the Australian region. *Mon. Wea. Rev.*, **133**, 3644–3660.
- Pu, Z., X. Li, C. Velden, S. Aberson, and W. T. Liu, 2008: Impact

- of aircraft dropsonde and satellite wind data on numerical simulations of two landfalling tropical storms during the Tropical Cloud Systems and Processes Experiment. *Wea. Forecasting*, **23**, 62–79.
- Rogers, E., T. Black, B. Ferrier, Y. Lin, D. Parrish, and G. DiMego, 2001: Changes to the NCEP Meso Eta analysis and forecast system: Increase in resolution, new cloud microphysics, modified precipitation assimilation, and modified 3DVAR analysis. NWS Tech. Procedures Bull. 488, NOAA/NWS. [Available online at <http://www.emc.ncep.noaa.gov/mmb/mmbpll/eta12tpb>.]
- Rogers, R., and Coauthors, 2006: The intensity forecasting experiment: A NOAA multiyear field program for improving tropical cyclone intensity forecasts. *Bull. Amer. Meteor. Soc.*, **87**, 1523–1537.
- Skamarock, W. C., J. B. Klemp, J. Dudhia, D. O. Gill, D. M. Barker, W. Wang, and J. G. Powers, 2005: A description of the Advanced Research WRF Version 2. NCAR Tech. Note NCAR/TN-468+STR, June 2005, 88 pp.
- Wang, Y., 2002: An explicit simulation of tropical cyclones with a triply nested movable mesh primitive equation model: TCM3. Part II: Model refinements and sensitivity to cloud microphysics parameterization. *Mon. Wea. Rev.*, **130**, 3022–3036.
- Willoughby, H. E., 1988: The dynamics of the tropical cyclone core. *Aust. Meteor. Mag.*, **36**, 183–191.
- , 1995: Mature structure and evolution. *Global Perspective on Tropical Cyclones*, WMO/TD 693, Rep. TCP-38, R. L. Elsberry, Ed., World Meteorological Organization, 21–62.
- , and P. G. Black, 1996: Hurricane Andrew in Florida: Dynamics of a disaster. *Bull. Amer. Meteor. Soc.*, **77**, 543–549.
- , H.-L. Jin, S. J. Lord, and J. M. Piotrowicz, 1984: Hurricane structure and evolution as simulated by an axisymmetric, nonhydrostatic numerical model. *J. Atmos. Sci.*, **41**, 1169–1186.
- Zehr, R. M., 2003: Environmental vertical wind shear with Hurricane Bertha (1996). *Wea. Forecasting*, **18**, 345–356.
- Zhu, T., and D.-L. Zhang, 2006: Numerical simulation of Hurricane Bonnie (1998). Part II: Sensitivity to varying cloud microphysical processes. *J. Atmos. Sci.*, **63**, 109–126.
- , —, and F. Weng, 2004: Numerical simulation of Hurricane Bonnie (1998). Part I: Eyewall evolution and intensity change. *Mon. Wea. Rev.*, **132**, 225–241.